Excited States and Reduced Transition Probabilities in ^{168}Os

T. Grahn,[1,2,*] S. Stolze,[2] D. T. Joss,[1] R. D. Page,[1] B. Sayğı,[1,†] D. O'Donnell,[1] M. Akmali,[1] K. Andgren,[3] L. Bianco,[1] D. M. Cullen,[4] A. Dewald,[5] P. T. Greenlees,[2] K. Heyde,[6] H. Iwasaki,[5] U. Jakobsson,[2] P. Jones,[2] D. S. Judson,[1] R. Julin,[2] S. Juutinen,[2] S. Ketelhut,[2] M. Leino,[2] N. Lumley,[4] P. J. R. Mason,[4,7] O. Möller,[8] K. Nomura,[5,9] M. Nyman,[2] A. Petts,[1] P. Peura,[2] N. Pietralla,[8] Th. Pissulla,[5] P. Rahkila,[2] P. J. Sapple,[1] J. Sarén,[2] C. Scholey,[2] J. Simpson,[7] J. Sorri,[2] P. D. Stevenson,[10] J. Uusitalo,[2] H.V. Watkins,[1] and J. L. Wood[11]

[1]*Department of Physics, Oliver Lodge Laboratory, University of Liverpool, Liverpool, L69 7ZE, United Kingdom.*
[2]*University of Jyvaskyla, Department of Physics, P.O. Box 35, FI-40014, University of Jyvaskyla, Finland.*
[3]*Department of Physics, Royal Institute of Technology, SE-10691, Stockholm, Sweden.*
[4]*Department of Physics and Astronomy, University of Manchester, Manchester M13 9PL, United Kingdom.*
[5]*Institut für Kernphysik, Universität zu Köln, 50937 Köln, Germany.*
[6]*Department of Physics and Astronomy, Ghent University, Proeftuinstraat 86, B-9000 Gent, Belgium.*
[7]*STFC Daresbury Laboratory, Daresbury, Warrington, WA4 4AD, United Kingdom.*
[8]*Institut für Kernphysik, TU Darmstadt, 64289 Darmstadt, Germany.*
[9]*Department of Physics, University of Tokyo, Hongo, Bunkyo-ku, Tokyo 113-003, Japan.*
[10]*Department of Physics, University of Surrey, Guildford, Surrey, GU2 7XH, United Kingdom.*
[11]*School of Physics, Georgia Institute of Technology, Atlanta, Georgia 30332-0430, USA.*

(Dated: November 17, 2016)

The level scheme of the neutron-deficient nuclide ^{168}Os has been extended and mean lifetimes of excited states have been measured by the recoil distance Doppler-shift method using the JUROGAM γ-ray spectrometer in conjunction with the IKP Köln plunger device. The ^{168}Os γ rays were measured in delayed coincidence with recoiling fusion-evaporation residues detected at the focal plane of the RITU gas-filled separator. The ratio of reduced transition probabilities $B(E2;4_1^+ \rightarrow 2_1^+)/B(E2;2_1^+ \rightarrow 0_1^+)$ is measured to be 0.34(18), which is very unusual for collective band structures and cannot be reproduced by IBM-2 model calculations based on the SkM* energy-density functional.

PACS numbers: 21.10.Tg, 21.10.Ky, 23.20.Lv, 27.70.+q

I. INTRODUCTION

The emergence of collective behavior in atomic nuclei outside closed shell configurations represents one of the most important paradigms in the description of many-body quantum mechanical systems [1, 2]. The systematics of excited states reveal fundamental information about the evolution of nuclear structure [3]. The largest range of isotopes between consecutive magic numbers that can be synthesised and studied in their excited states is found within the $82 \leq N \leq 126$ shell. The longest continuous chain with known excited states is for osmium, which spans 37 isotopes from ^{162}Os ($N = 86$) [4] to ^{198}Os ($N = 122$) [5]. The Os excitation energy systematics $E(4_1^+)/E(2_1^+)$ show the development from single-particle excitations near the $N = 82$ closed shell [4, 6], through soft triaxial rotors ($N \sim 92$) [7] and shape coexistence ($N = 96$) [8, 9] towards well-deformed prolate shapes near the midshell at $N = 104$. Beyond $N = 104$ collectivity decreases towards $N = 126$ due to the diminishing valence space [5, 10, 11], see Fig. 1(a).

Reduced transition probabilities, particularly $B(E2)$ values, serve as a more sensitive experimental probe for analyzing collectivity as a function of nucleon number. The $B(E2)$ values usually increase with spin for low-lying states within a rotational band [2]. A consequence of this feature is that the $B(E2;4_1^+ \rightarrow 2_1^+)/B(E2;2_1^+ \rightarrow 0_1^+)$ ratio (hereafter known as $B_{4/2}$) is larger than unity for collective excitations, 1.43 and 2.0 for an ideal rotor and vibrator, respectively. However, in nuclei near closed shells where single-particle motion dominates the nuclear structure, this increasing trend of the $B(E2)$ values can be reversed [12]. Ten nuclei with $B_{4/2}$ ratios less than unity were identified in a survey of reduced transition probability ratios [13]. Although some of the cases have been re-measured using complementary experimental techniques and the anomaly rectified (e.g. ^{98}Ru and ^{180}Pt) [14], the anomaly persists in several other nuclei, such as ^{114}Xe and ^{114}Te [15, 16]. Further anomalous cases have since been reported, including ^{72,74}Zn [17] and ^{48,50}Cr [18].

This paper reports an extension to the level scheme in ^{168}Os and the measurement of mean lifetimes of excited states using the recoil distance Doppler-shift (RDDS) method. The anomalously low value for the $B_{4/2}$ ratio deduced from the measurements cannot be reproduced by IBM-2 model calculations based on the SkM* energy-

*Electronic address: tuomas.grahn@jyu.fi
†Department of Physics, Faculty of Science, Ege University, Bornova, Izmir, 35100, Turkey.

TABLE I: Summary of reactions employed in the present work. The data from experiments 1 and 2 were used for the γ-ray coincidence analysis, while those from experiment 3 were used for the lifetime measurements.

Experiment	Beam Species	Beam Energy (MeV)[a]	Average beam current (pnA)	Target Isotope	Thickness (mg/cm^2)	Exit Channel	Residual Nucleus	Irradiation time (h)
1	^{78}Kr^{15+}	335	7	^{92}Mo	0.5	2p	^{168}Os	162
2	^{78}Kr^{15+}	348	7	^{92}Mo	0.5	2p	^{168}Os	48
3	^{78}Kr^{15+}	345	3	^{92}Mo	1.0	2p	^{168}Os	160

[a]Bombarding energy at the front of the target.

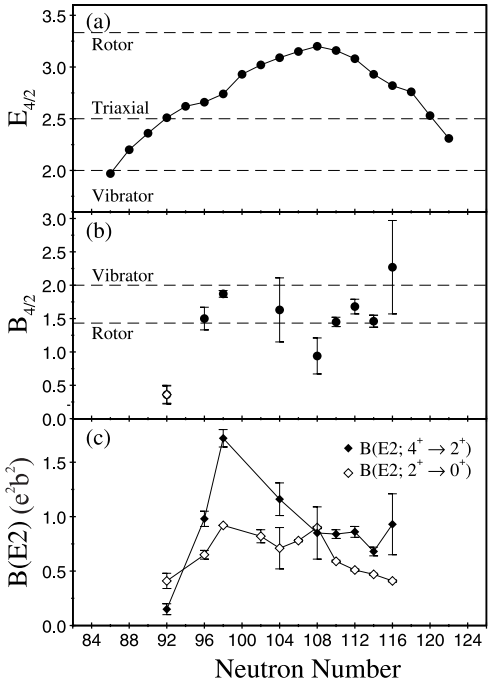

FIG. 1: (a) Ratios of the 4^+ to 2^+ state excitation energies for the even-mass Os isotopes. (b) Ratios of the reduced transition probabilities ($B_{4/2}$) measured for the even-mass Os isotopes. (c) Measured reduced transition probabilities B(E2) for the $4^+ \rightarrow 2^+$ (filled diamonds) and $2^+ \rightarrow 0^+$ (open diamonds) transitions. The measured values for ^{168}Os correspond to neutron number $N = 92$. Data for the heavier isotopes were obtained from Ref. [19].

density functional.

II. EXPERIMENTAL DETAILS

Excited states of ^{168}Os were populated in the fusion-evaporation reactions in experiments performed at the Accelerator Laboratory of the University of Jyväskylä listed in Table I. In each experiment γ rays were detected with the JUROGAM γ-ray spectrometer consisting of 43 Eurogam Phase I-type escape-suppressed spectrometers [20] arranged in six angular groups with respect to the beam direction. Evaporation residues recoiling from the target were separated in flight from unreacted beam and fission fragments according to their magnetic rigidity by the RITU gas-filled separator [21] before being implanted into the GREAT spectrometer [22] located at the focal plane. Recoiling fusion residues were distinguished from background events by their energy loss in the GREAT multiwire proportional counter and, in conjunction with the GREAT double-sided silicon strip detectors (DSSDs), their time-of-flight characteristics. These data were recorded using the Total Data Readout data acquisition system [23] and analyzed offline using the GRAIN [24] and RADWARE software packages [25]. All γ-ray data were recorded in delayed coincidence with fusion-evaporation residues implanted into the GREAT spectrometer.

In experiments 1 and 2 a high-fold coincidence analysis was performed leading to a significant extension of the ^{168}Os level scheme. In experiment 3 the standard JUROGAM target chamber was replaced by the IKP Köln plunger device [26], in which the distance between the target and a degrader foil was varied. This allowed lifetimes to be measured for excited states using the RDDS method. The stretched self-supporting ^{92}Mo target had a thickness of 1 mg/cm^2 while the degrader was a 1 mg/cm^2 thick Mg foil. The reaction provided a recoil velocity of $v/c = 3.8\%$ and 2.8% before and after the degrader, respectively.

III. RESULTS

A. $\gamma\gamma\gamma$ coincidence analysis

A total of 9.3×10^6 recoil-γ^n ($n \geq 3$) coincidences were recorded in the combined data from experiments 1 and 2 and sorted into an $E_{\gamma1} - E_{\gamma2} - E_{\gamma3}$ coincidence cube. The level scheme for ^{168}Os was constructed on the basis of relative γ-ray intensities and coincidence relationships. The deduced level scheme for ^{168}Os is displayed in Fig. 2 and the properties of γ rays assigned to this nucleus are recorded in Table II.

Gamma-ray transitions in ^{168}Os were first identified using the recoil-decay tagging technique and a high spin level scheme was established [7]. In the present work the aligned $\nu i_{13/2}{}^2$ band (band 2) has been extended from the (18^+) state by two transitions. The negative-parity

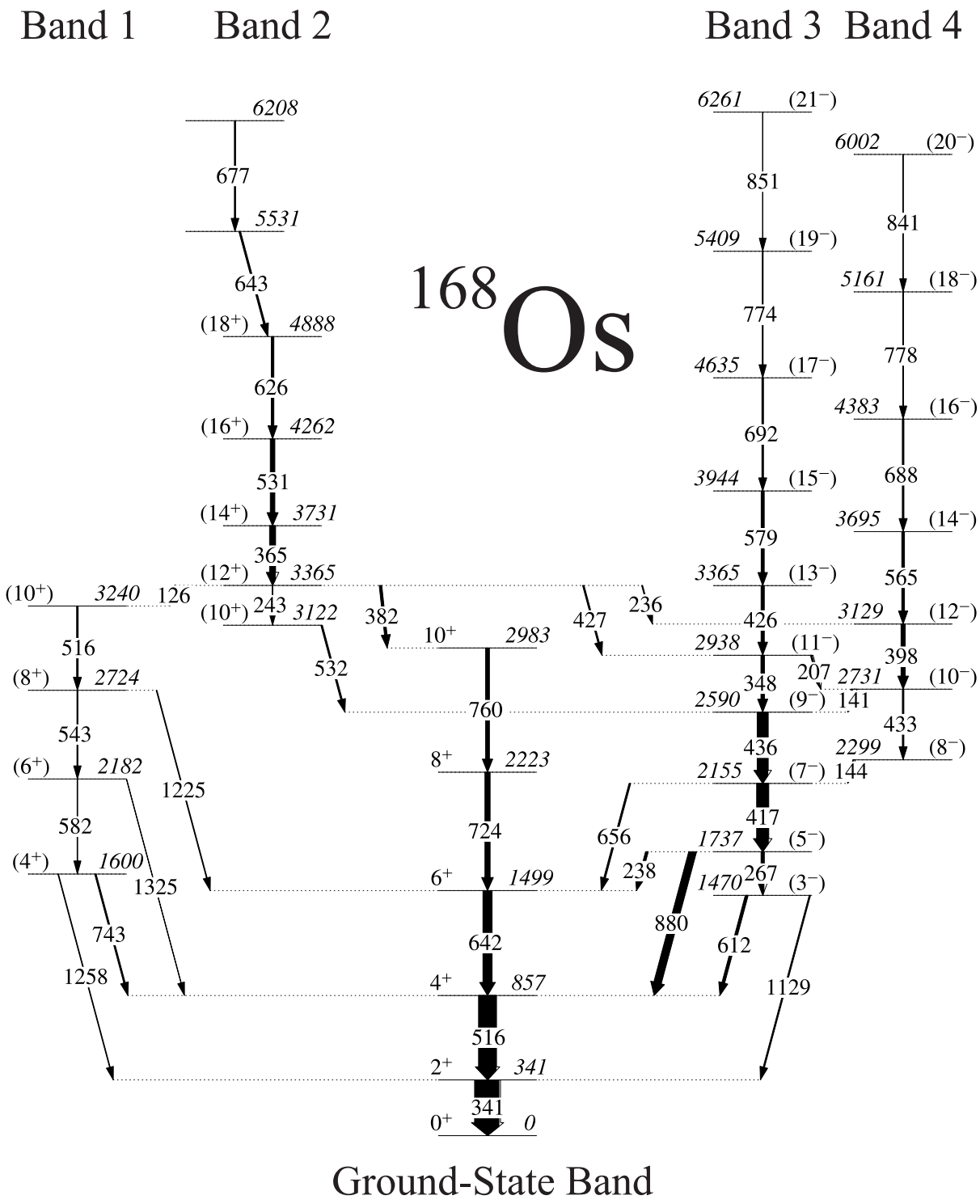

FIG. 2: Level scheme deduced for ^{168}Os. The transition energies are given in keV and their relative intensities are proportional to the widths of the arrows. Excited states are labelled with their excitation energies relative to the ground state and their spin and parity assignments. Parentheses indicate tentative assignments.

TABLE II: Measured properties of γ-ray transitions assigned to ^{168}Os. Energies are accurate to $\pm$0.5 keV for the strong (I_γ >10%) transitions rising to $\pm$2.0 keV for the weaker transitions.

E_γ (keV)	I_γ (%)	E_i (keV)	I_i		I_f
125.8	1.97(15)	3365	(12^+)	$\rightarrow$	(10^+)
140.5	7.6(5)	2731	(10^-)	$\rightarrow$	(9^-)
144.5	3.3(3)	2299	(8^-)	$\rightarrow$	(7^-)
207.0	6.1(4)	2938	(11^-)	$\rightarrow$	(10^-)
236.1	3.8(3)	3365	(12^+)	$\rightarrow$	(12^-)
237.6	10.6(7)	1737	(5^-)	$\rightarrow$	6^+
243.3	2.31(18)	3365	(12^+)	$\rightarrow$	(10^+)
267.0	12.0(8)	1737	(5^-)	$\rightarrow$	(3^-)
341.1	100(7)	341	2^+	$\rightarrow$	0^+
348.4	13.6(9)	2938	(11^-)	$\rightarrow$	(9^-)
365.4	23.5(15)	3731	(14^+)	$\rightarrow$	(12^+)
382.3	10.1(7)	3365	(12^+)	$\rightarrow$	10^+
398.3	16.5(10)	3129	(12^-)	$\rightarrow$	(10^-)
417.3	48(3)	2155	(7^-)	$\rightarrow$	(5^-)
426.0	12.7(9)	3365	(13^-)	$\rightarrow$	(11^-)
426.8	5.9(5)	3365	(12^+)	$\rightarrow$	(11^-)
432.7	6.0(5)	2731	(10^-)	$\rightarrow$	(8^-)
435.5	44(3)	2590	(9^-)	$\rightarrow$	(7^-)
515.5	6.2(6)	3240	(10^+)	$\rightarrow$	(8^+)
516.3	72(5)	857	4^+	$\rightarrow$	2^+
531.1	18.3(12)	4262	(16^+)	$\rightarrow$	(14^+)
531.9	6.3(6)	3122	(10^+)	$\rightarrow$	(9^-)
542.6	3.8(4)	2724	(8^+)	$\rightarrow$	(6^+)
565.5	10.8(7)	3695	(14^-)	$\rightarrow$	(12^-)
579.1	12.2(8)	3944	(15^-)	$\rightarrow$	(13^-)
582.0	2.2(3)	2182	(6^+)	$\rightarrow$	(4^+)
590.8	4.4(4)	3713		$\rightarrow$	(10^+)
612.2	11.5(8)	1470	(3^-)	$\rightarrow$	4^+
625.8	10.4(7)	4888	$(18^+$	$\rightarrow$	(16^+)
641.8	37.2(24)	1499	6^+	$\rightarrow$	4^+
643.1	6.8(5)	5531	(20^+)	$\rightarrow$	(18^+)
656.3	6.7(5)	2155	(7^-)	$\rightarrow$	6^+
677.3	4.8(3)	6208	(22^+)	$\rightarrow$	(20^+)
688.1	6.5(5)	4383	(16^-)	$\rightarrow$	(14^-)
691.9	6.4(5)	4635	(17^-)	$\rightarrow$	(15^-)
724.1	21.1(14)	2223	8^+	$\rightarrow$	6^+
743.4	5.8(6)	1600	(4^+)	$\rightarrow$	4^+
760.1	15.5(10)	2983	10^+	$\rightarrow$	8^+
774.0	3.4(3)	5409	(19^-)	$\rightarrow$	(17^-)
778.2	3.3(3)	5161	(18^-)	$\rightarrow$	(16^-)
840.8	1.04(15)	6002	(20^-)	$\rightarrow$	(18^-)
851.2	1.35(16)	6261	(21^-)	$\rightarrow$	(19^-)
879.9	31.3(20)	1737	(5^-)	$\rightarrow$	4^+
1128.8	5.3(5)	1470	(3^-)	$\rightarrow$	2^+
1224.8	3.0(3)	2724	(8^+)	$\rightarrow$	6^+
1257.7	2.7(5)	1600	(4^+)	$\rightarrow$	(4^+)
1325.2	1.5(3)	2182	(6^+)	$\rightarrow$	4^+

bands (bands 3 and 4) are similarly extended to the (21^-) and (20^-) states by two and one transitions, respectively. Figure 3 shows typical double-gated spectra highlighting these extensions of the ^{168}Os level scheme. Band 2 in Fig. 2, is fed by a 643 keV transition that is unresolved

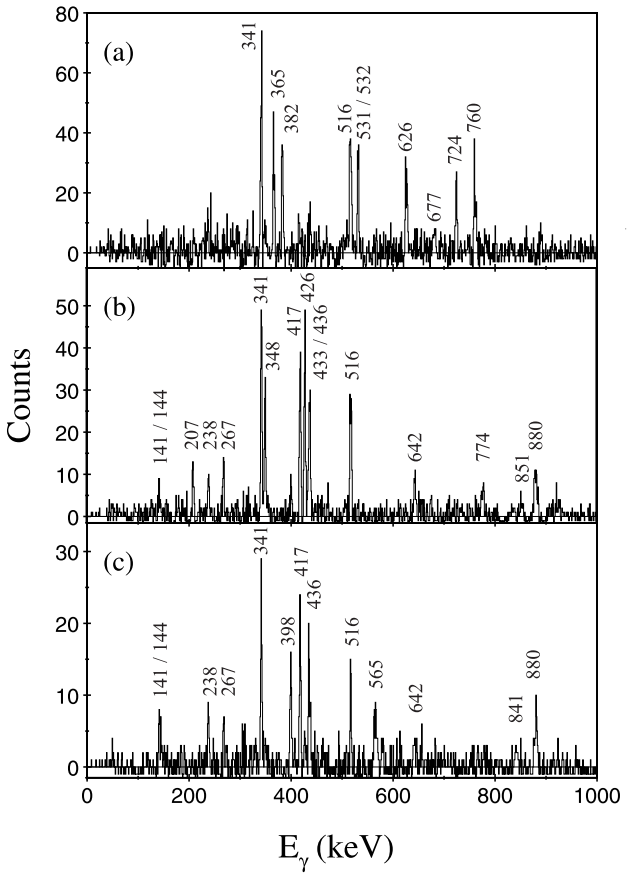

FIG. 3: Double-gated γ-ray coincidence spectra correlated with a recoil implantation in the GREAT spectrometer. (a) spectrum showing γ rays in coincidence with the 642 and 643 keV transitions. (b) Spectrum showing γ rays in coincidence with the 579 and 692 keV transitions in band 3. (c) Spectrum showing γ rays in coincidence with the 688 and 778 keV transitions in band 4.

from the 642 keV ($6_1^+ \rightarrow 4_1^+$) transition in the ground-state band. Figure 3 (a) shows γ rays in coincidence with both 642 and 643 keV transitions and supports the placement of the 643 keV γ-ray transition feeding band 2. Figures 3 (b) and (c) show typical coincidence spectra used to extend bands 3 and 4, respectively.

The (12^+) state in band 2 was known previously to have discrete γ-ray branches to the ground-state band and the negative-parity side bands, bands 3 and 4. Two further depopulation paths from the (12^+) state have been established, see Fig. 2. The 243 keV and the 532 keV transitions feed band 3, while the 126 keV transition feeds a new band structure, band 1. It was not possible to measure the multipolarities of the transitions in the new band. However, a positive-parity even-spin structure is inferred from the nature of the γ-ray transition branches to the low-spin states of the ground-state band. The spectra highlighting these decay paths are shown in Figs. 4 and 5. The 591 keV transition in Fig. 4 (b) appears to feed the level at 3122 keV.

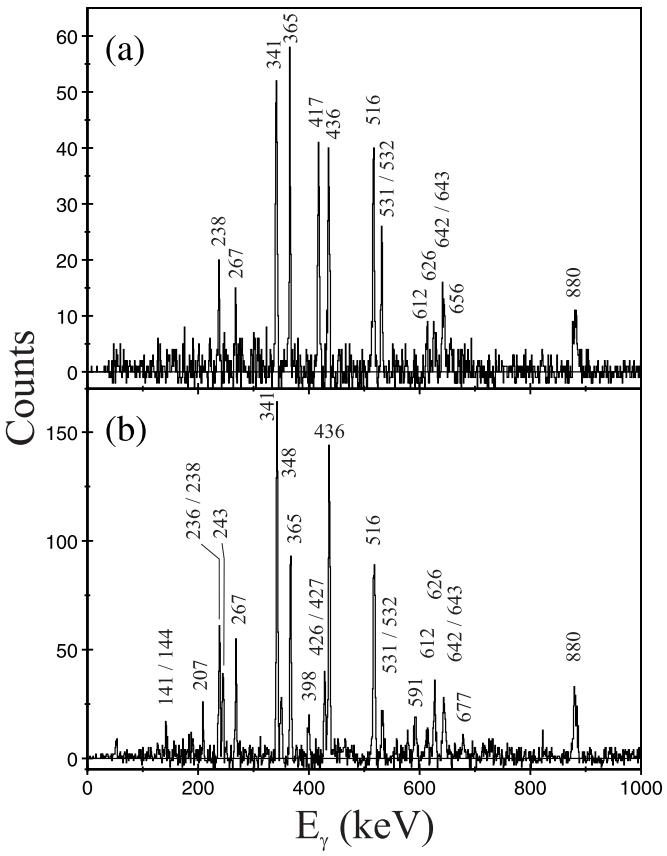

FIG. 4: Double-gated γ-ray coincidence spectra correlated with a recoil implantation in the GREAT spectrometer. Spectra providing evidence for a new decay path from the (12^+) state to the 9^- state in Band 3. (a) spectrum showing γ rays in coincidence with the 243 and 532 keV transitions that connect band 2 with band 3. (b) Spectrum showing γ rays in coincidence with the 531 keV/532 keV and 417 keV transitions.

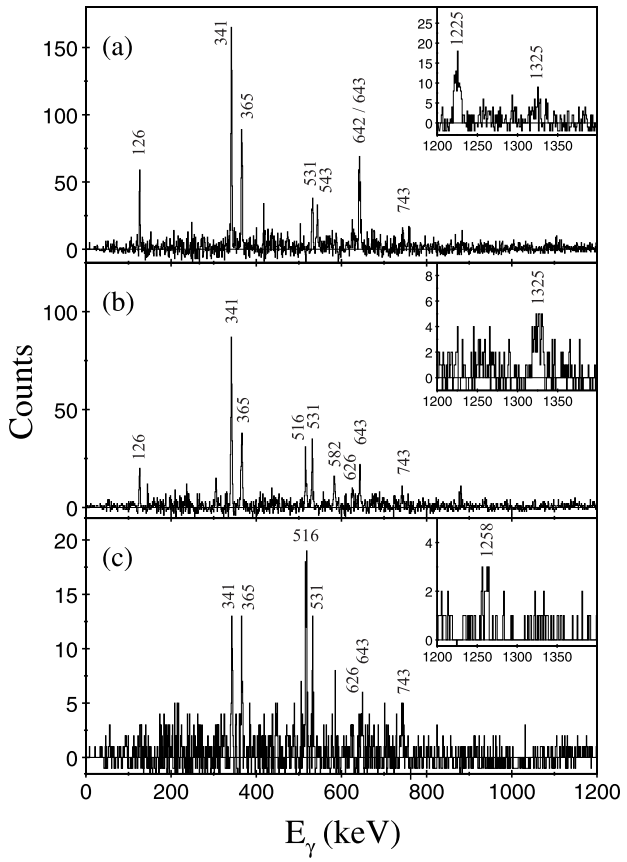

FIG. 5: Double-gated γ-ray coincidence spectra correlated with a recoil implantation in the GREAT spectrometer. Spectra show a new decay path from the (12^+) state to Band 1. Insets to the figure show the high-energy linking transitions from Band 1 to the ground-state band. (a) spectrum showing γ rays in coincidence with both transitions of the 516 keV doublet. (b) Spectrum showing γ rays in coincidence with the 516 and 543 keV transitions. (c) Spectrum showing γ rays in coincidence with the 543 and 582 keV transitions.

B. RDDS lifetime measurements

Recoil-correlated γ-ray coincidences were recorded at 13 different target-to-degrader distances of the plunger device for $\sim$12 hours each. The experiment was optimized for the lifetime measurements of the 2^+ and 4^+ states, i.e. the distances were chosen to span a region of sensitivity where the relative intensities of the fully shifted and degraded components of the depopulating transitions for these states varied, see Fig. 6. The recoil-gated γ-ray coincidences were analyzed in order to eliminate the influence of unobserved feeding transitions on the lifetimes under investigation [27].

Sufficient γ-ray data were collected with JUROGAM at the detector angles of 158° (5 detectors) and 134° (10 detectors) in coincidence with the γ rays recorded with all the detectors to allow the measurements of the 2^+ and 4^+ state lifetimes using the Differential Decay Curve Method (DDCM) [28]. In the DDCM mean lifetimes are obtained from the relative intensity variation with distance of the fully Doppler-shifted and degraded components of the γ-ray transitions feeding and depopulating the level of interest through the Equation

$$\tau = \frac{Q^d_{\rm depop}(x) - Q^d_{\rm feed}(x)}{v\frac{d}{dx}[Q^s_{\rm depop}(x)]}, \qquad (1)$$

where $Q^i_j(x) = I^i_j/(I^s_j + I^d_j)$ and $I^i_j(x)$ are the γ-ray intensities for the shifted ($i = s$) and degraded ($i = d$) components measured at the target-to-degrader distance x for the depopulating ($j =$ depop) and feeding ($j =$ feed) transitions, respectively. Therefore, the γ-ray intensities I recorded with different distances x are normalized by the sum of their fully shifted and degraded components. The final lifetime is an error-weighted average of individual lifetimes (Eq. 1) obtained at different target-to-degrader distances within the region of sensitivity where the derivative of the decay curve is greater than zero.

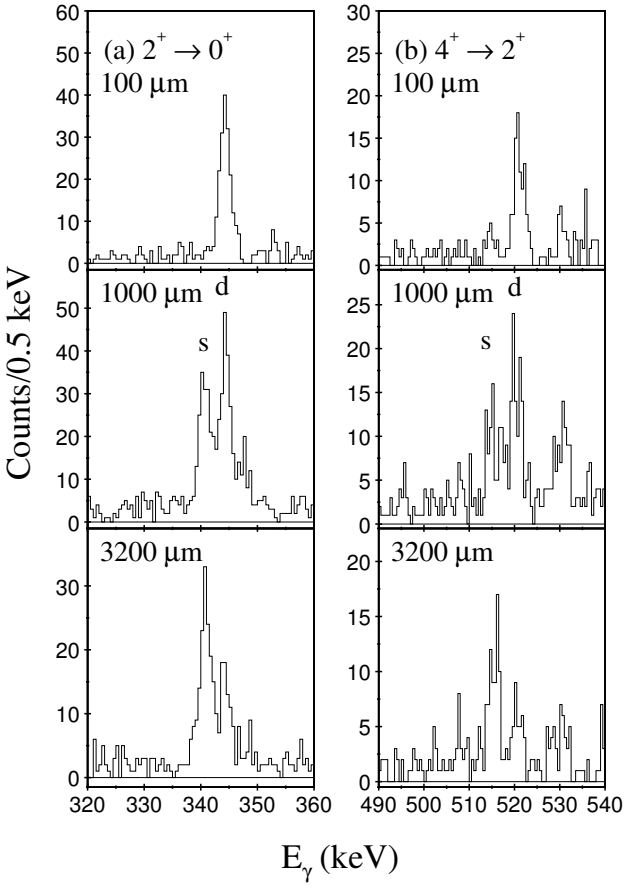

FIG. 6: Recoil-gated $\gamma\gamma$ coincidence spectra of ^{168}Os recorded at three different target-to-degrader distances with five JUROGAM Ge detectors at 158°. (a) Gamma rays in coincidence with the 516 keV $4_1^+ \rightarrow 2_1^+$ transition (b) Gamma rays in coincidence with the 642 keV $6_1^+ \rightarrow 4_1^+$ transitions. The fully Doppler-shifted (s) and degraded (d) components of the 341 keV and 516 keV γ-ray transitions are labeled.

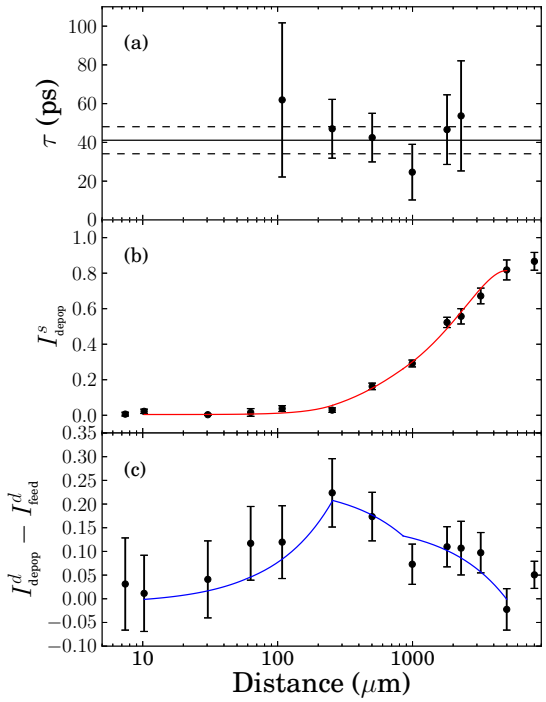

FIG. 7: Lifetime determination using the Differential Decay Curve Method (DDCM). (a) The individual mean lifetimes determined within the region of sensitivity [28] and the final mean lifetime and error bar as the solid and dashed horizontal lines, respectively. (b) The decay curve for the 2^+ state extracted from the coincidence spectra gated directly above the states under investigation and recorded with five Ge detectors at 158°. The line drawn through the experimental points is the fit of the decay curve. (c) The numerator of Eq. 1 and the derivative of the decay curve.

Lifetime determination for the 2^+ and 4^+ states are as shown in Figs. 7 and 8, respectively.

In order to obtain statistically viable γ-ray spectra, coincidences were demanded between the full line shape of the 516 keV ($4^+ \rightarrow 2^+$) and 642 keV ($6^+ \rightarrow 4^+$) direct feeding transitions, recorded with the whole JUROGAM array, and the depopulating transitions recorded with the JUROGAM detectors at 158° or 134°, in order to extract the lifetimes of the 2^+ and 4^+ states, respectively. In order to extract directly feeding γ-ray intensities, gates were set below the states of interest. Examples of recoil-gated $\gamma\gamma$-coincidence spectra are shown in Fig. 6 and decay curves are shown in Figs. 7 and 8. The present variant of DDCM, in which the full line shape is used for gating, has been used and discussed in references [27, 29]. The standard DDCM procedure, in which gates are set on the fully shifted components of the transitions of interest was impossible in the present case due to the limited statistics in the $\gamma\gamma$-coincidence spectra.

The lower intensities of the higher-lying transitions precluded lifetime measurements using $\gamma\gamma$ coincidences. Instead these lifetimes were obtained using γ-ray singles data correlated with recoil implantations followed within 6.3 s by a characteristic α decay of ^{168}Os [30] in the same DSSD pixel. The influence of the unobserved feeding transitions on the lifetime of interest cannot be eliminated when extracting lifetimes from singles γ-ray spectra, so it was assumed that the time behavior of the observed and unobserved feeding was similar [27, 31].

The present work establishes that the 642 and 516 keV transitions are self-coincident doublets, see Fig. 2. However, a significant influence of the 643 keV transition on the extracted lifetimes can be ruled out based on the fact that weak degraded components were observed below these high-lying doublet transitions as shown in Fig. 9 for the 642 keV transition. This implies that the 626 keV transition and all the preceding ones in the cascade are fast compared to the transitions under investigation. As defined by Eq. 1, the feeding intensity is determined by the degraded component and therefore the time be-

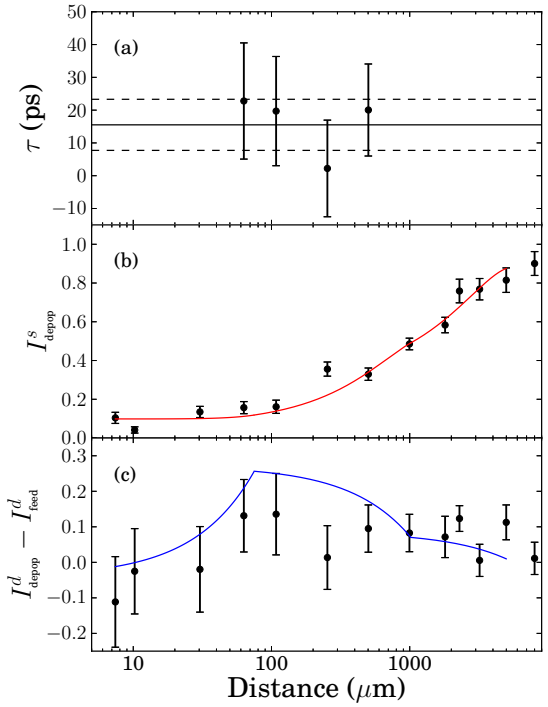

FIG. 8: Lifetime determination using the Differential Decay Curve Method (DDCM). (a) The individual mean lifetimes determined within the region of sensitivity [28] and the final mean lifetime and error bar as the solid and dashed horizontal lines, respectively. (b) The decay curve for the 4^+ state extracted from the coincidence spectra gated directly above the states under investigation and recorded with five Ge detectors at 158°. The line drawn through the experimental points is the fit of the decay curve. (c) The numerator of Eq. 1 and the derivative of the decay curve.

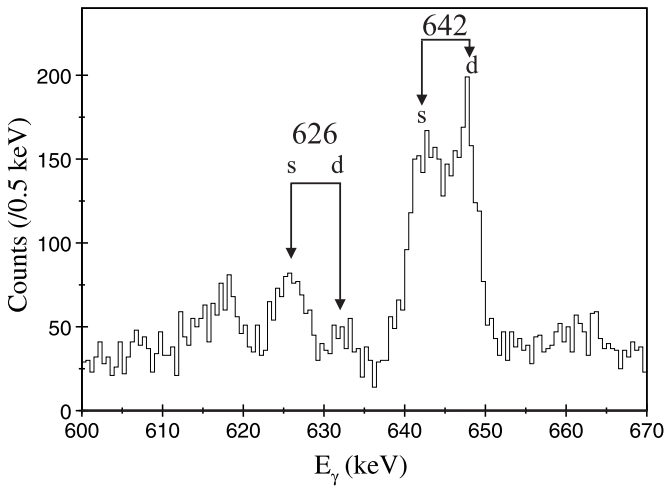

FIG. 9: Sum of γ-ray spectra at 158° for all target-to-degrader distances. The γ-ray energies are Doppler corrected using the initial recoil velocity. The fully shifted (s) component of the 626 keV transition is much stronger than its degraded (d) counterpart, which should lie at around 6 keV higher in energy. In contrast, the fully shifted and degraded components of the 642 keV peak have comparable intensities. This comparison indicates that the lifetime of the 626 keV and its preceding transitions are shorter lived.

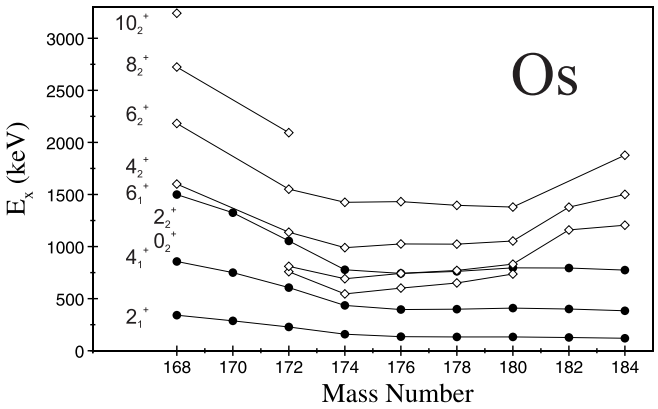

FIG. 10: Energy levels in the ground-state band (filled circles) and excited positive-parity structure (unfilled circles) as a function of mass number. The data are labelled by their assigned spins and parities. Data for the $A \geq 170$ Os isotopes are taken from reference [34].

havior of the doublet transitions do not interfere with the current DDCM analysis. Furthermore, the relative intensity of the 515.5 keV transition (Table 2) is less than 10% of that of 516.3 keV transition and thus any influence falls within the statistical error bars of the extracted lifetime.

Table III lists the measured mean lifetimes τ, reduced transition probabilities $B(E\lambda)$ and the absolute values for the transition dipole (D_t) and quadrupole (Q_t) moments.

IV. DISCUSSION

A. The excited positive-parity structure.

Band 1 is assigned to be a positive-parity structure that forms one of the decay paths from the (12^+) state in band 2. Similar decay paths to positive-parity bands have been observed in nearby nuclei such as ^{156}Dy [32] and ^{158}Er [33]. Excited positive-parity bands have been observed in the heavier even-N Os isotopes than ^{170}Os in experiments probing non-yrast states populated in the β decay of the odd-odd Ir precursors [9, 34]. Figure 10 compares band 1 in ^{168}Os with the systematic trends established for the heavier isotopes. These trends resemble those established for the W isotopes by Kibédi *et al.*, who found that the states in the first excited positive-parity bands have a parabolic energy dependence on neutron number [35].

TABLE III: Electromagnetic properties of ^{168}Os extracted from the present work.

I^π	τ (ps)	$I_i^\pi \to I_f^\pi$	E_γ (keV)	$B(E2)$ (e^2b^2)	$B(E2)$ (W.u.)	$\lvert Q_t\rvert$ (eb)	$B(E1)$ (10^{-3}W.u.)	$\lvert D_t\rvert$ ($10^{-3}e$b$^{1/2}$)
2^+	41(7)	$2^+ \to 0^+$	341.1	0.41(7)	74(13)	4.5(4)		
4^+	16(8)	$4^+ \to 2^+$	516.3	0.14(7)	25(13)	2.2(6)		
(12^+)	740(50)	$(12^+) \to 10^+$	382.3	0.0048(4)	0.86(6)	0.37(3)		
		$(12^+) \to (10^+)$	125.8	0.24(2)	43(3)	2.6(2)		
		$(12^+) \to (10^+)$	243.3	0.0105(7)	1.90(13)	0.55(4)		
		$(12^+) \to (12^-)$	236.1				0.0068(5)	0
		$(12^+) \to (10^-)$	426.8				0.00074(5)	0.36(3)
(14^+)	17(2)	$(14^+) \to (12^+)$	365.4	0.70(9)	130(15)	4.5(3)		
(5^-)	59(7)	$(5^-) \to (3^-)$	267.0	0.22(3)	40(5)	3.2(4)		
		$(5^-) \to 4^+$	879.9				0.0045(6)	1.6(2)
		$(5^-) \to 6^+$	237.6				0.076(9)	7.1(9)
(7^-)	21(4)	$(7^-) \to (5^-)$	417.3	0.26(3)	48(5)	4.2(4)		
		$(7^-) \to 6^+$	656.3				0.0064(7)	2.2(3)

B. Reduced transition probabilities and moments

The measured intra-band $B(E2)$ values can be related to the transition quadrupole moment Q_t through the equation

$$B(E2; I_i \to I_f) = \frac{5}{16\pi} e^2 Q_t^2 \langle I_i 020 | I_f 0\rangle^2. \quad (2)$$

Similarly, the measured $B(E1)$ values can be expressed in terms of the transition dipole moment D_t with the relation

$$B(E1; I_i \to I_f) = \frac{3}{4\pi} D_t^2 \langle I_i 010 | I_f 0\rangle^2. \quad (3)$$

Equations 2 and 3 hold for an axially symmetric rotating nucleus with $K = 0$. Although these relations are not exact for the transitional case where non-axial degrees of freedom are expected to occur, the quantities $|Q_t|$ and $|D_t|$ can be regarded as parameters in the context of the present work, in which they will be used for systematic comparisons. The $B(E2)/B(E1)$ branches for the negative-parity states have been extracted from the measured lifetimes using the relative γ-ray intensities given in Table II. The $B(E1)$ transition probabilities for transitions from the (7^-) and (9^-) states in band 3 are large (see Table III) and support their interpretation as an octupole vibrational band at low frequency.

C. The $B(E2; 4_1^+ \to 2_1^+)/B(E2; 2_1^+ \to 0_1^+)$ ratio.

The smooth variation of the $E_{4/2}$ ratio between the vibrational and rotational regimes belies an intriguing feature in the reduced transition probabilities of ^{168}Os$_{92}$. Figure 1 (b) shows the variation of the $B_{4/2}$ ratio as a function of neutron number for the Os isotopes. The measured ratios extracted for the $N \geq 96$ isotopes indicate values that are typical of rotational nuclei. The $B_{4/2}$ ratios reflect the tendency of $B(E2)$ values to increase as a function of spin within a rotational band structure at low spin, as generally predicted in collective models [36]. The ratio deduced for ^{168}Os, $B_{4/2} = 0.34(18)$, shows a marked deviation from the heavier isotopes and seems to suggest a remarkably low collectivity of the $4_1^+ \to 2_1^+$ transition compared with the $2_1^+ \to 0_1^+$ transition, see Fig. 1(c). In an extreme case if ^{168}Os were an axially symmetric rotor, one would expect a $B_{4/2} = 1.43$, which for the measured 2^+ lifetime would require a 4^+ state lifetime of $\tau \approx 3.5$ ps.

This striking behavior was not anticipated in theoretical calculations for ^{168}Os. Previous calculations include a QCD-inspired relativistic energy-density functional approach [37] in which systematic ground-state deformations across isotopic chains were compared with experimental values derived from $B(E2)$ values [38]. No sudden change in deformation was predicted at $N = 92$ in these calculations although a small discontinuity was present at $N = 98$. Smoothly varying behavior was also predicted by other theoretical approaches including a number-projected BCS model [39] and a QRPA description based on realistic interactions [40].

In this work, spectroscopic calculations of the excited state energies and absolute $B(E2)$ values have been performed within the proton-neutron interacting boson model (IBM-2) [41]. The parameters of IBM-2 were determined by mapping the potential energy surface, calculated by a constrained Hartree-Fock plus BCS (HF+BCS) calculation [42] with the Skyrme SkM* (or the "modified SkM") interaction [43], onto the classical limit of the IBM-2 Hamiltonian. Details of the calculation technique can be found in Refs. [44, 45]. The proton and neutron effective charges were set to be equal and fixed at $e_\pi = e_\nu = 0.12$ eb by the comparison between the intrinsic quadrupole moments obtained from the HF+BCS calculation and the IBM-2 model. It should be noted that the following result does not depend on the choice of the interaction at the qualitative level, as the topology of the potential energy surface around the global minimum remains unchanged. This is confirmed by the fact that both the Skyrme SkM* and the SLy4 in-

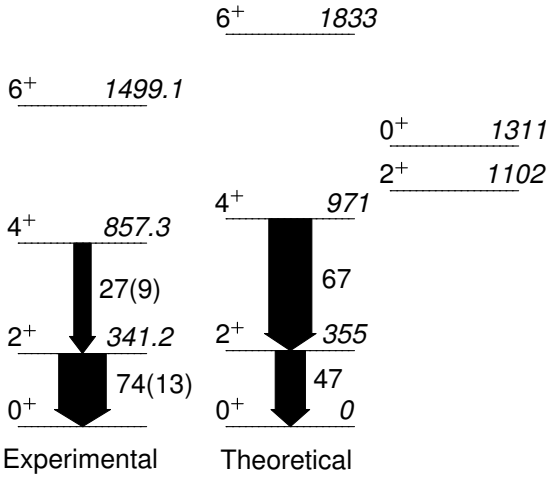

FIG. 11: Comparison of experimental and theoretical results of the present study. The level energies are given in keV. The width of the arrows are proportional to the $B(E2)$ values, which are given next to the arrows in W.u.

teractions predict the same β_2 deformation value on the prolate axis and similar collective patterns are predicted by the mapped IBM. The comparison between the hybrid SkM*-IBM and the experimental data is shown in Fig. 11. The energy levels are reasonably well reproduced in the ground-state band but the theoretical calculations predict $B(E2)$ values that follow the characteristic trend of a rotational band that do not agree with the measurements.

There are two known circumstances in which a sudden loss of collectivity in a ground-state band can occur. The first is in a seniority dominated structure where the $B(E2; 2_1^+ \rightarrow 0_1^+)$ strength reflects a $\nu = 2 \rightarrow \nu = 0$ $E2$ transition and the $B(E2; 4_1^+ \rightarrow 2_1^+)$ strength reflects a $\nu = 2 \rightarrow \nu = 2$ $E2$ transition [46] where ν is the seniority quantum number. Generally, seniority structures are only known to occur at and near to closed shells, and possibly at subshells [47, 48]. This mechanism is thought to be unlikely for the anomaly in ^{168}Os since its N and Z are rather far from magicity and sub-shell gaps are not expected.

The second scenario for a lower collectivity arises from shape coexistence where the $B(E2; 2_1^+ \rightarrow 0_1^+)$ strength reflects an intra-band $E2$ transition and the $B(E2; 4_1^+ \rightarrow 2_1^+)$ strength reflects an inter-band $E2$ transition as observed in nuclei such as ^{184}Hg [49]. The main reservation for attributing the anomaly to coexisting intruder structures is that such features generally only appear in regions near to closed shells for protons and near mid-shell (or near a subshell) for the neutrons or vice versa [3]. Furthermore, band-mixing calculations for ^{168}Os suggest that the deformed intruder band head in ^{168}Os lies at an excitation energy around 1.8 MeV [7].

The excited positive-parity structure (band 1) observed in this work might provide an alternative candidate for mixing with the yrast states. Figure 11 shows the IBM-2 predictions for the excitation energies of the β ($K^\pi = 0^+$) and γ ($K^\pi = 2^+$) band heads at 1311 keV and 1102 keV, respectively. The predicted 0_2^+ state lies at an energy consistent with extrapolations of the measured energy level systematics shown in Fig. 10. The calculations suggest that mixing with the non-yrast states is not sufficient to account for the anomalous $B_{4/2}$ ratios. Thus, it seems unlikely that the anomalous $B(E2)$ values arise from mixing with coexisting states. However ^{168}Os has a $E_{4/2}$ ratio that is consistent with that expected for a transitional γ-soft nucleus, see Fig. 1(a), so shape fluctuations may give rise to significant mixing but calculating th is beyond the scope of this work.

V. CONCLUSIONS

The level scheme for ^{168}Os has been extended in a γ-ray coincidence experiment using the JUROGAM spectrometer used in conjunction with the RITU gas-filled separator and the GREAT focal plane spectrometer. Recoil distance Doppler-shift lifetime measurements using the differential decay curve method have been performed in a complementary experiment using these devices in conjunction with the IKP Köln plunger. The particularly small $B(E2; 4_1^+ \rightarrow 2_1^+)/B(E2; 2_1^+ \rightarrow 0_1^+)$ ratio deduced for ^{168}Os could not be reproduced using IBM-2 model calculations based on the SkM* energy-density functional. This anomaly appears unlikely to arise from seniority or shape coexistence phenomena. Further work is required to investigate whether the expected triaxiality of ^{168}Os might contribute to this unusual observation.

Acknowledgments

This work has been supported through EURONS (European Commission contract no. RII3-CT-2004-506065), the Academy of Finland under the Finnish Centre of Excellence Programme 2006-2011 (Nuclear and Accelerator Based Physics contract 213503) and the UK Science and Technology Facilities Council. The UK/France (STFC/IN2P3) Loan Pool and GAMMAPOOL network are acknowledged for the EUROGAM detectors of JUROGAM. TG, PTG and CS acknowledge the support of the Academy of Finland, contract numbers 131665, 111965 and 209430, respectively. Financial support (KH) from the "FWO-Vlaanderen" and the InterUniversity Attraction Pole Programme, Belgian State Federal Office for Scientific, Technical and Cultural Affairs (IAP Grant No P7/12) is acknowledged.

[1] A. Bohr and and B.R. Mottelson, *Nuclear Structure Volume 1: Single-Particle Motion* (W. A. Benjamin Inc, New York, USA, 1969).

[2] A. Bohr and and B.R. Mottelson, *Nuclear Structure Volume 2: Nuclear Deformation* (W. A. Benjamin Inc, New York, USA, 1975).

[3] K. Heyde and J. L. Wood, Rev. Mod. Phys. **83**, 1467 (2011).

[4] D. T. Joss *et al.*, Phys. Rev. C **70**, 017302 (2004).

[5] Z. Podolyak *et al.*, Phys. Rev. C **79**, 031305(R) (2009).

[6] M. C. Drummond *et al.*, Phys. Rev. C **87**, 054309 (2013).

[7] D. T. Joss *et al.*, Nucl. Phys. A **689**, 631 (2001).

[8] J. L. Durell, G. D. Dracoulis, C. Fahlander and A. P. Byrne, Phys. Lett. B **115**, 367 (1982).

[9] P. M. Davidson, G. D. Dracoulis, T. Kibedi, A. P. Byrne, S. S. Anderssen, A. M. Baxter, B. Fabricius, G. J. Lane and A. E. Stuchbery, Nucl. Phys. A **568**, 90 (1994).

[10] C. Wheldon *et al.*, Nucl. Phys. A **699**, 415 (2002), ISSN 0375-9474.

[11] P. D. Bond, R. F. Casten, D. D. Warner and D. Horn, Phys. Lett. B **130**, 167 (1983).

[12] A. de Shalit and I. Talmi, *Nuclear Shell Theory* (Academic Press, New York, 1963).

[13] R. B. Cakirli, R. F. Casten, J. Jolie, and N. Warr, Phys. Rev. C **70**, 047302 (2004).

[14] E. Williams *et al.*, Phys. Rev. C **74**, 024302 (2006).

[15] G. de Angelis *et al.*, Phys. Lett. B **535**, 93 (2002), ISSN 03702693.

[16] O. Möller *et al.*, Phys. Rev. C **71**, 064324 (2005).

[17] C. Louchart *et al.*, Phys. Rev. C **87**, 0543902 (2013).

[18] D. Hertz-Kintish, L. Zamick and S.J.Q. Robinson, Phys. Rev. C **90**, 034307 (2014).

[19] Data extracted using the NNDC On-Line Data Service from the ENSDF database, file revised as of 22.2.2010. M. R. Bhat, Evaluated Nuclear Structure Data File (ENSDF), Nuclear Data for Science and Technology, page 817, edited by S. M. Qaim (Springer- Verlag, Berlin, Germany, 1992).

[20] C. W. Beausang *et al.*, Nucl. Instrum. Methods Phys. Res. A **313**, 37 (1992).

[21] M. Leino *et al.*, Nucl. Instrum. Methods Phys. Res. B **99**, 653 (1995).

[22] R. D. Page *et al.*, Nucl. Instrum. Methods Phys. Res. B **204**, 634 (2003).

[23] I. H. Lazarus *et al.*, IEEE Trans. Nucl. Sci. **48**, 567 (2001).

[24] P. Rahkila, Nucl. Instrum. Methods Phys. Res. A **595**, 637 (2008).

[25] D. C. Radford, Nucl. Instrum. Methods Phys. Res. A **361**, 297 (1995).

[26] L. Cleemann *et al.*, Nucl. Instrum. Methods **156**, 477 (1978).

[27] T. Grahn *et al.*, Phys. Rev. C **80**, 014324 (2009).

[28] A. Dewald, S. Harissopulos, and P. von Brentano, Z. Phys. A **334**, 163 (1989).

[29] A. Dewald *et al.*, Phys. Rev. C **68**, 034314 (2003).

[30] R. D. Page, P. J. Woods, R. A. Cunningham, T. Davinson, N. J. Davis, A. N. James, K. Livingston, P. J. Sellin and A. C. Shotter., Phys. Rev. C **53**, 660 (1996).

[31] M. Scheck, T. Grahn, A. Petts, P. A. Butler, A. Dewald, L. P. Gaffney, M. B. G. Hornillos, A. Görgen, P. T. Greenlees, K. Helariutta, et al., Phys. Rev. C **81**, 014310 (2010).

[32] M. A. Riley *et al.*, Nucl. Phys. A **486**, 456 (1988).

[33] T. S. Dinoko *et al.*, Eur. Phys. J. A **63**, 01005 (2013).

[34] T. Kibedi, G. D. Dracoulis, A. P. Byrne and P. M. Davidson, Nucl. Phys. A **567**, 183 (1994).

[35] T. Kibedi, G. D. Dracoulis, A. P. Byrne, and P. M. Davidson, Nucl. Phys. A **688**, 669 (2001).

[36] D. J. Rowe and J. L. Wood, *Fundamentals of nuclear models: foundational models*, vol. 1 (World Scientific, 2009).

[37] P. Finelli, N. Kaiser, D. Vretenar, and W. Weise, Nuclear Physics A **770**, 1 (2006), ISSN 03759474.

[38] S. Raman, C. W. Nestor, and P. Tikkanen, At. Data Nucl. Data Tables **78**, 1 (2001).

[39] N. Benhamouda *et al.*, in *AIP Conference Proceedings* (AIP, 2009), vol. 1090, p. 613.

[40] S. Peltonen, D. Delion, and J. Suhonen, Physical Review C **71** (2005).

[41] T. Otsuka *et al*, Nucl. Phys. A **309**, 1 (1978).

[42] P. Bonche *et al*, Compt. Phys. Commun. **171**, 49 (2005).

[43] J. Bartel *et al.*, Nucl. Phys. A **386**, 79 (1982).

[44] K. Nomura *et al*, Phys. Rev. Lett. **101**, 142501 (2008).

[45] K. Nomura *et al*, Phys. Rev. C **81**, 044307 (2010).

[46] J. J. Ressler *et al.*, Phys. Rev. C **69**, 034317 (2004).

[47] P. Van Isacker and S. Heinze, Phys. Rev. Lett. **100**, 052501 (2008).

[48] K. Sieja, F. Nowacki, K. Langanke, and G. Martínez-Pinedo, Phys. Rev. C **79**, 064310 (2009).

[49] W. C. Ma *et al.*, Phys. Lett. **167B**, 277 (1986).